# Control and Power Management of a 24-Hour DC Microgrid Improved Model

Elie Hleihel, Maurice Fadel, Hadi y Kanaan

# Control and Power Management of a 24-Hour DC Microgrid Improved Model

Elie Hleihel[1,2], Maurice Fadel[1,] and Hadi Y. Kanaan[2]
[1]Université de Toulouse, LAPLACE, 2 rue Charles Camichel 31071 Toulouse Cedex 7
[2]Saint-Joseph University of Beirut, Faculty of Engineering – ESIB, Mar Roukoz, Mkalles, Beirut, Lebanon
hleihel@laplace.univ-tlse.fr, maurice.fadel@laplace.univ-tlse.fr, hadi.kanaan@usj.edu.lb

***Abstract*- In recent decades, the microgrid concept emerged as a solution to electrify remote areas and integrate renewable energy sources to mitigate environmental pollution. Owing to the evolution of power electronic devices, the ease of control, and the improved efficiency and reliability, DC microgrids are gaining increased interest. Many kinds of research address the hierarchical control in DC microgrids to accomplish multi-objectives. On the first and second levels, the control targets fast dynamic variables to achieve its objectives. Yet, on a third control level, general management functionalities are executed. Many of these management functionalities target the system variables with a slower dynamic and so, to prove the effectiveness of the proposed hierarchical control, a 24-hour model simulation is required. The wide time-range dynamics of the existing system variables make the 24-hour modeling subject a complicated matter especially, on standard computers with conventional performances. To overcome this problem, this paper proposes a 24-hour DC microgrid model which offers the best tradeoff between model precision, complexity, and simulation speed. The multi-objectives hierarchical control is adopted: on a first and second control level, several averaging techniques are introduced and compared to a detailed reference model in terms of accuracy and calculation step size. DC microgrid's general management strategy is adopted on the third control level. Simulation tests are performed on MATLAB/Simulink software to prove the viability of the proposed 24-hour model.**

## I. INTRODUCTION

Back to the beginning of the 21st century and throughout the last decades, the microgrid concept has arisen rapidly and spread all around the world. Microgrids consist of a variety of interconnected energy sources that can be divided into traditional pollutant sources such as coal, oil, natural gas, etc., and renewable energy sources (RESs) such as solar, wind energy sources.

Even though (RESs) constitute sustainable and friendly environmental alternatives to pollutant energy sources for the future of energy production, it imposes new challenges and impediments in terms of stability, reliability, and energy quality due to its different and intermittent nature [1]. Initially, most of the studies were focusing on AC microgrids in terms of configuration, control, stability, and optimization because of the maturity, reliability, and standardization of the AC technology. Afterward, the DC technology emerged which diverted extensively the research to the DC microgrids. The traditional AC microgrids hierarchal control is adopted as a strategy to control DC microgrids and is divided into three

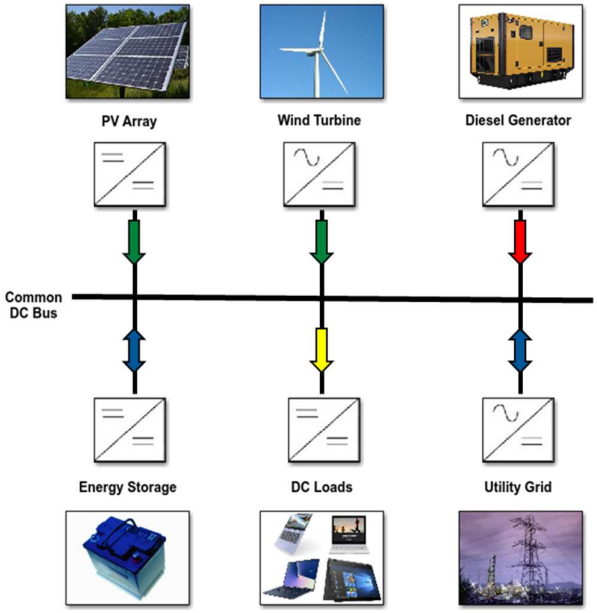


Fig.1 DC microgrid typical configuration

levels: the first level includes all basic functions such as droop control, or current and voltage loops, etc. The second level consists of source depending functions such as MPPT algorithms, state of charge estimation of energy storage systems ( ESSs), and the third level includes decentralized coordinated functions such DC bus signaling (DBS), or power line signaling (PLS), and global microgrid level energy management functions [2]. Besides the difference of functionalities, in each of the three levels of the hierarchical control, these control levels differ as well in time scales. Hence, the time constants of each control level are defined based on the dynamic response of the corresponding system variables and inputs. The wide span in time constants makes the simultaneous application of multi-objectives control levels practically tough in one simulation model. Therefore, many surveys adopting the hierarchical control strategy seek to achieve nearby time range objectives.

In [3] the traditional droop control is adopted as a primary control; a secondary control level is added to improve its robustness and ensure proper power-sharing while a tertiary control level accomplishes global energy management

functions such controlling the power flow of microgrid or enhancing the efficiency of the conversion system. The effectiveness of the proposed hierarchical control is proved in a simulation time range of tens/hundreds of seconds.

However, adopting the hierarchical control on a 24-hour DC microgrid model to achieve realistic power management functions remains a complicated matter. In fact, none of standard PC with a high processor and installed memory performance can model a 24-hour DC microgrid, including the switching devices of power electronics which operate in the range of tens/hundreds of microseconds along with realistic load profiles which vary on an hourly basis. Particularly, the hardware in the loop setup (HIL) using real-time digital simulators can achieve a 24-hour horizon simulation with the best precision because of their advanced computational speed and capacities.

In absence of high performant servers, averaging techniques and simplified mathematical models of existing DC microgrid units and power electronics devices are applied. By this, the fast-dynamic variables are excluded from the system which can degrade the model accuracy and leads to dynamic and static power accounting errors. An explicit compromise between the model precision and model complexity exists.

Thereby, this paper proposes an improved 24-hour DC microgrid model to cope with the abovementioned modeling problematic. It ensures the best trade-off between model precision, model complexity, and simulation speed. The proposed model is tested on a standard core i7 computer processor and is compared to a reference instantaneous model [4]. The rest of this paper is organized as follows: In section II, the 24-hour DC microgrid modeling strategy is presented. Each source is modeled apart with its conversion chain and obtained models are compared to the reference ones in terms of accuracy and simulation speed. In section III, the DC microgrid power management strategy is detailed. Simulation tests consisting of realistic scenarios are performed in section IV to prove the viability of the proposed model. Finally, section V concludes the paper.

## II. 24-HOUR DC MICROGRID MODELLING STRATEGY

Fig.1 shows a typical DC microgrid configuration to be adopted in the frame of this work. It consists of renewable energy sources (RESs): a solar PV array and a wind turbine, a lithium-ion battery as an ESS, a back-up diesel generator as a pollutant source, and DC loads. The adopted DC microgrid can operate in an islanded mode as well as in grid-connected mode to either buy or sell energy to the utility grid. All microgrid units are connected to the common DC bus through converters. Each converter is controlled locally based on a well-defined strategy of control.

On a first and second control level, all RESs are functioning in maximum power point tracking (MPPT) mode to extract maximum available power, the battery takes charge of stabilizing the common DC bus to ensure microgrid stable operation, the diesel generator and the utility grid are (PQ) controlled and are connected intermittently to the microgrid based on the power management strategy to be extended in section III. MATLAB/Simulink software is utilized to model the DC microgrid. Furthermore, in all accomplished simulations, the ode23tb (Stiff\TR-BDF2) variable-step solver along with the Simulink accelerator mode are selected due to their high performance in increasing the simulation speed for long-time simulations. It is worth it to mention that the proposed DC microgrid model is built on Simulink and all modeling equations are referred to as "Simscape" "Specialized Power Systems" library. In the following, each microgrid unit is modeled apart with its conversion chain:

### *A. PV Array*

The PV array conversion chain consists of a PV array block connected to the common DC bus through a DC/DC boost converter which is controlled in MPPT mode to extract maximum available power. PV array block equations are derived from the *"PV Array" "SimScape"* library block. The P-*V* characteristic for a PV array is defined by equation (1):

$$P(V_{PV}) = \mathrm{I_{PV}} \times \mathrm{V_{PV}} \quad (1)$$
$$P(V_{PV}) = \mathrm{V_{PV}} \times I_L - \mathrm{V_{PV}} \times \mathrm{I_0}\left[exp\left(\frac{V_{PV}+\mathrm{R_s}.\mathrm{I_{PV}}}{V_T}\right) - 1\right] - \mathrm{V_{PV}} \times I_{sh}$$

Where $I_{PV}, I_L, I_0, V_d, V_T, I_{sh}, V_{PV}$ and $R_s$ are respectively: PV current (A), light generated current(A), diode saturation current (A), diode voltage (V), temperature voltage (V),shunt resistance current (A), PV voltage (V) and series resistance ($\Omega$). The irradiation in ($W/m^2$) and the temperature in (℃) are inputs of the PV array block. The PV array block is modeled as a variable current source connected to DC/DC boost, considered as a current source converter (CSC). The DC/DC boost electrical circuit diagram is illustrated in Fig.2. Hence, average model equations are deduced as follows:

$$C_{in}\frac{dV_{PV}}{dt} = I_{PV} - I_L \quad (2)$$
$$V_L = V_{Bus}.(1-D) \quad (3)$$
$$L\frac{dI_L}{dt} = V_{PV} - V_L - R_L.I_L \quad (4)$$
$$I_{pv_{out}} = (V_L.I_L)/V_{Bus} \quad (5)$$

Where $C_{in}$,, $L$, $D$ , $I_L$, $V_L$, $R_L$, $I_{pv_{out}}$ and $V_{Bus}$ are respectively source side capacitor, converter inductor, duty cycle ratio, inductor current, converter controlled- voltage source, inductor

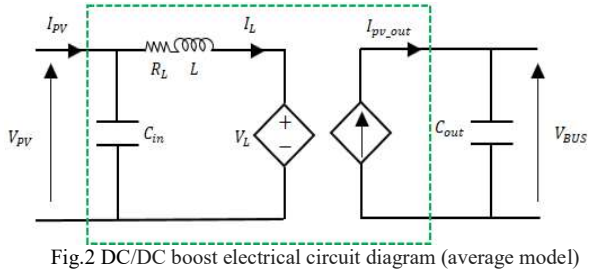

Fig.2 DC/DC boost electrical circuit diagram (average model)

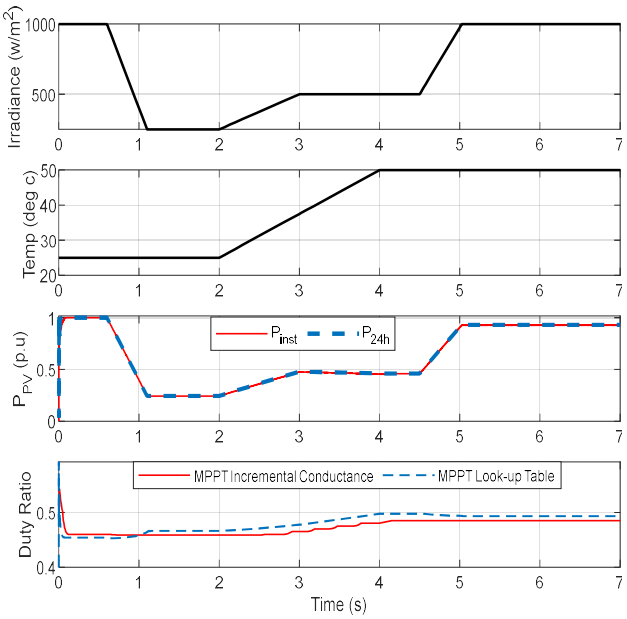


Fig.3 Comparison of proposed 24-hour PV and instantaneous models

resistance, converter controlled- current source, and common DC bus voltage. Knowing that most MPPT existing techniques require small sampling times to converge which limits the solver maximum step size and slows-down the simulation, an MPPT look-up table method is adopted to increase simulation speed. As a principle, for each temperature and irradiation inputs combination, a PV output voltage reference, corresponding to the maximum power point extraction, exists. The PV voltage real value is regulated to track its reference through a series P.I (P.I parameters are listed in table 1). The proposed PV configuration (Fig.2.a) is compared to the instantaneous one [4]. Variable temperature and irradiation inputs are applied, and the results are shown in Fig.3. Both, instantaneous and 24-hour PV models, have the same power curves in transient as well as in steady-state. Based on the duty cycle ratio plots, the MPPT proposed look-up table keeps a good accuracy (maximum 1.5% error) as the incremental conductance adopted in the instantaneous model. Furthermore, the simulation speed is highly increased in the proposed 24-hour model. As the instantaneous model includes the switching devices, the simulation speed is imperatively limited by the switching frequency ($f_s = 10$ kHz). Thus, the instantaneous model calculation step size is limited at $T_{step_{inst}} = 1\,\mu s$ , to obtain precise results whereas, in the 24-hour model a much higher calculation step size is obtained $T_{step_{24h}} = 41.7\,ms$. Consequently, the PV 24-hour proposed model highly improves the simulation speed by reducing the calculation step size without losing any of model accuracy.

### *B. Wind Turbine*

The applied wind turbine configuration is shown in fig.4. a. A wind turbine model takes as inputs the wind speed (m/s), the rotor speed (p.u), and the regulated pitch angle ($\beta$ in degrees) and outputs the torque applied to the generator shaft. The generator consists of a permanent magnet synchronous machine (PMSM) in a positive sequence phasor model [5]. We take note that the phasor solution method is proposed by MATLAB /Simulink to reduce the system complexity. This solution method computes sinusoidal electrical components as phasors in the vicinity of the (PMSM) fundamental nominal frequency ($f_n = 50\,Hz$). Higher components of frequencies spectrum are ignored which reduces notably the state-space model. As a result, electrical components are modeled by their magnitudes and phases instead of their sinusoidal waveforms which increases the calculation step size and so the simulation speed. Besides, machine electrotechnical oscillations inertia and regulators are still modeled, and the system keeps the same accuracy. As the (PMSM) produces three-phase AC power, it is connected to the common DC bus via a three-phase rectifier. Fig.4. b shows the Simulink block diagram of wind turbine $(dq)$ power control: (PMSM) outputs the three-phase current phasors $(\overline{I_{abc}})$ and the rotor rotational speed $(w_r)$. $i_{dq}$ are obtained throughout a complex to $(dq)$ transformation. The optimal torque MPPT method is adopted and generates a power electrical reference corresponding to the maximum power tracking. The resulting electrical power reference is compared to the real value $(P_{elec})$ which is computed as follows:

$$P_{elec} = \frac{3}{2}\left(V_d.i_d + V_q.i_q\right) \qquad (6)$$

Where $V_d, V_q, i_d,$ and $i_q$ are respectively d- axis voltage component, q- axis voltage component, d- axis current component, and q- axis current component. $P_{elec}$ is regulated through a P.I controller. The P.I output sets the d-axis current reference $i_{d\_ref}$ while the reactive power is controlled by the q-axis current reference which is set to zero $(i_{q\_ref} = 0)$ to absorb zero reactive power. Inner $(dq)$ current (P.I) regulators are applied and a system linearization is required to generate the positive sequence voltage $(V_{dq})$ (P.I parameters are listed in table 1). The converter control phasor voltages are computed $(\overline{V_{abc}}_{Ctrl\_conv})$. Due to the phasor modeling and in absence of any sinewave voltage representation, the three- phase rectifier average model can simply be modeled by a gain of $(\frac{V_{BUS}}{2})$ where $V_{BUS}$ is the common DC bus voltage. By this, (PMSM) stator phasor voltages are deduced $(\overline{V_{abc}}_{stator})$. More details on the optimal torque MPPT method and the $(dq)$ control in wind turbine applications can be found in [6], [7]. In bellow a simulation test comparison of proposed 24-hour configuration and instantaneous model. Both models are tested on a 5 second time range under two winds speed different values:

- $0 < t < 3.6\,s$, $V = 12\,m/s$ corresponds to a maximum of mechanical power: $P_{mec\_MPPT} = 0.9\,p.u$ and a rotor speed of $\Omega = 1\,p.u$.

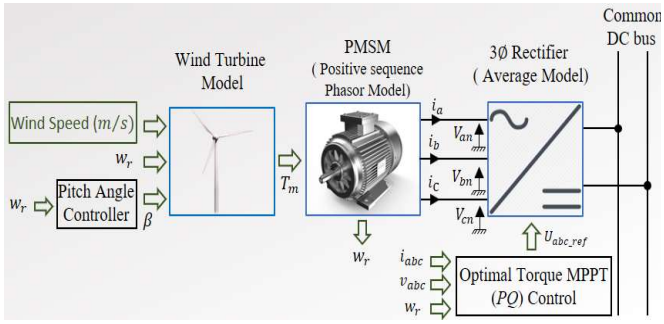


Fig.4.a Wind Turbine 24-Hour Model Configuration

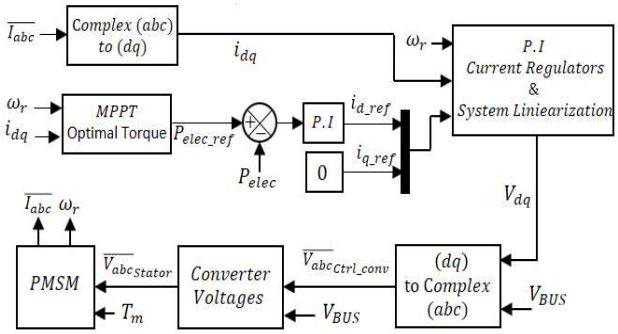


Fig.4.b Block diagram of wind turbine $(dq)$ power control

$-3.6 \leq t < 5\ s$, $V = 10.8\ m/s$ corresponds to $P_{mec\_MPPT} = 0.6561\ p.u$ and $\Omega = 0.9\ p.u$.

Simulation results are shown in Fig.5. a, and Fig.5.b show that the proposed 24-hour model curves are all combined with the instantaneous ones in transient as well in steady state.

In the first curve plot, a difference in mechanical and electrical power curves is visualized ($P_{mec} \neq P_{elec}$). It results from the (PMSM) efficiency. Electrical and mechanical (PMSM) detailed equations of the instantaneous model are changeless in the phasor model. Also, the rotor mechanical speed follows its maximum reference values ($\Omega = 1\ p.u$ when the input wind speed is equal 12m/s then it decreases to $\Omega = 0.9\ p.u$, corresponding to the MPPT). The Optimal torque MPPT technique converges and has the same results in both simulation models. Furthermore, $(dq)$ Current components are the same in both models, and $q$-axis current components (dashed red line and solid bold gold line) are set to zero, as predefined, to absorb zero reactive power. Fig.5.b validates the phasor model in which the voltage component is modeled by its magnitude and phase angle. The voltage magnitude of the phasor model follows the instantaneous and average sinewave voltages curves. Consequently, the 24-hour model still includes all (PMSM) electromechanical equations which make the application of the MPPT technique and inner current loops always valid and accurate. On the other hand, the simulation speed is increased significantly with the phasor modeling solution which highly reduces the CPU and RAM usages (the instantaneous model necessitates a calculation step size of

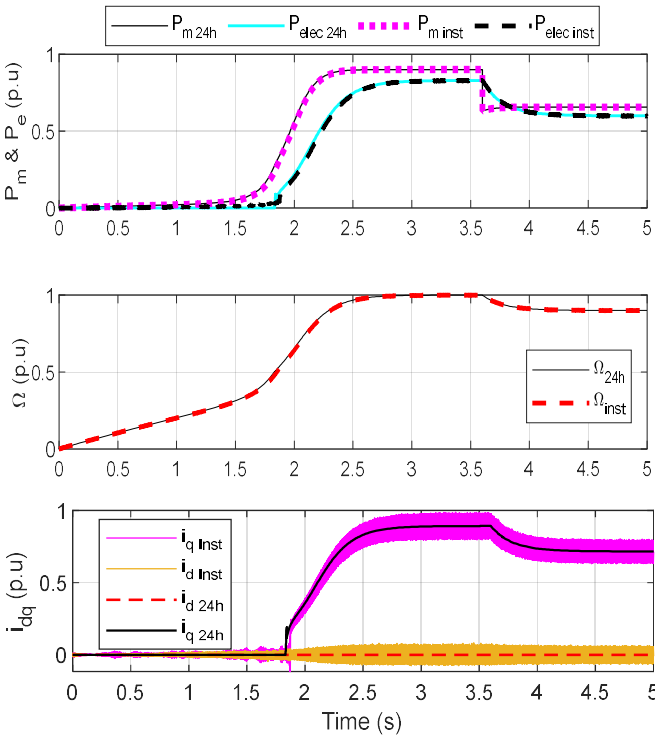


Fig.5.a Comparison of wind turbine proposed 24-hour and instantaneous models

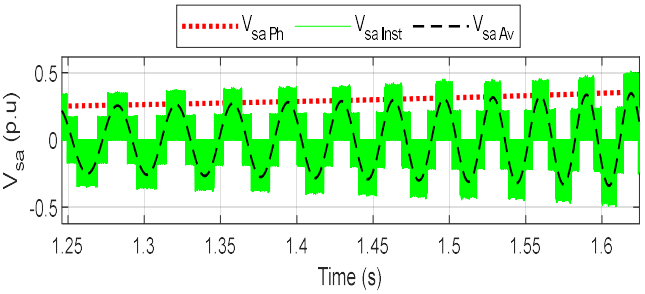


Fig.5.b Phase A stator voltage comparison in instantaneous (solid green line), average ( dashed black line) and phasor model (dotted red line)

$T_{step\_inst} = 0.8\ \mu s$ to yield well-shaped curves whereas the 24-hour model requires an average calculation step size of $T_{step\_24h} = 12.2\ ms$).

### C. *Diesel generator*

Different mathematical models of diesel generator (DG) are mentioned in [8]. The dynamic model adopted in this study addressees the electrical aspects of a (DG) rather than the mechanical ones. As shown in fig.6.a, it consists of a diesel engine modeled by a second-order transfer function, and a governor system modeled by a P.I.D. controller which regulates the generator speed on the desired value. This block outputs the diesel engine mechanical power to be provided to the simplified synchronous machine (SM). The (SM) electrical characteristic consists of a three phases AC system, each phase includes a voltage source in series with an RL impedance. The mechanical equation system is the same as the detailed (SM)

one. The electrical system strategy of control is depicted in Fiq.6. b. Similarly to the wind turbine configuration, the $(dq)$ control strategy is applied along with the phasor solution approach. $(dq)$ current components references are selected as follows: $d$-axis component $i_{d\_ref}$ is fixed by the third hierarchical control level, it can be null if the diesel generator is disconnected from the microgrid or equal to a predefined value, computed on the third control level ($P_{DG\_re} \neq 0$) if the (DG) is connected to the microgrid. Contrarily, $q$-axis component $i_{q\_ref}$ is always set to zero to absorb zero reactive power. Uniformly to previous units, a simulation test is carried out to prove the effectiveness of the (DG) 24-hour model. The results are listed in Fig.7. In all plots, the two models' curves are combined: the electrical power follows its reference and has the same curve as the $d$-axis current component, $q$-axis component is equal to zero and absorbs zero reactive power. Moreover, the (DG) governor regulates the rotational speed which remains constant and equal to the reference value ($\Omega = \Omega_{ref} = 1$ p. u). The same result as the wind turbine simulation is obtained in terms of simulation speed. Consequently, the 24-hour system effectiveness is verified. Uniformly, the utility grid model is identical to the (DG) electrical system which consists of three phases voltage sources with RL impedances.

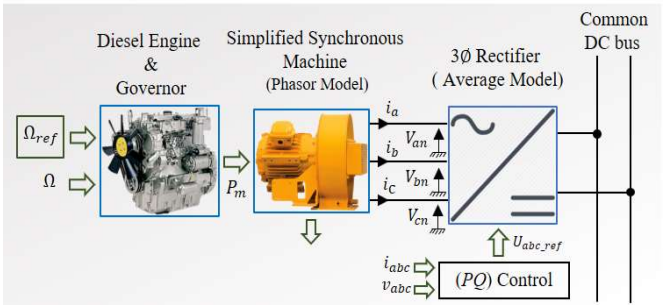


Fig.6.a Diesel generator 24-hour model configuration

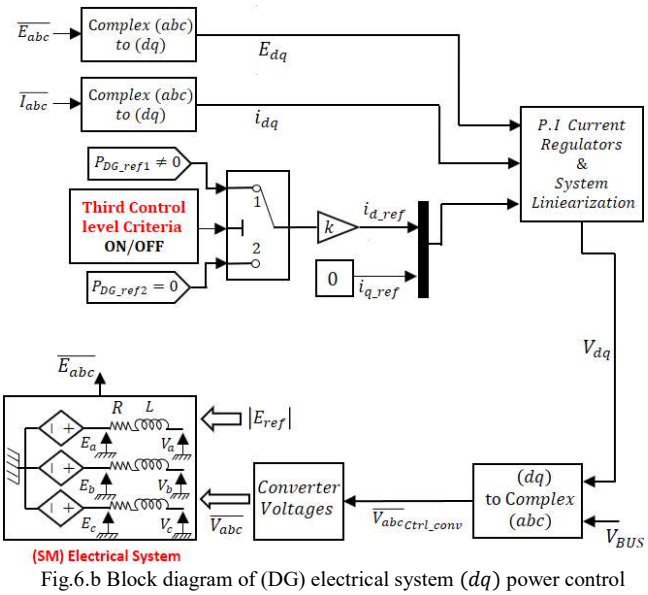


Fig.6.b Block diagram of (DG) electrical system $(dq)$ power control

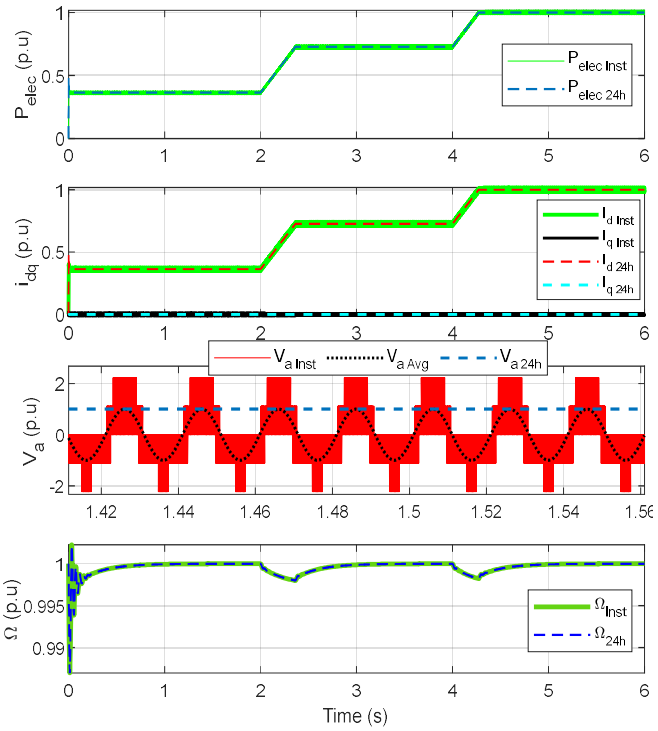


Fig.7 Comparison of (DG) proposed 24-hour and instantaneous models

(RLE) sources are connected to the common DC bus through a three phases rectifier. Furthermore, the same $(dq)$ control, depicted in Fig.6.b, is selected to manage the two possible microgrid functioning modes (grid-connected/islanded). Finally, a single distinction in $(dq)$ controller of both models is revealed: the reference power selected in grid-connected mode ($P_{grid\_ref1} \leftrightarrow P_{DG\_ref1}$) is set to a negative value if excess in microgrid's power is to be sold to the utility grid ($P_{grid\_ref1} < 0$), whereas it has a positive sign ($P_{grid\_ref1} > 0$) if a lack in microgrid's generated power needs to be recovered by buying electricity from the utility grid.

### *D. Battery and DC loads*

To model the energy storage system (ESS), a lithium-ion battery is implemented. This battery type is preferred because of its substantial efficiency and economic benefits [9]. To emulate the battery behavior, MATLAB/Simulink "Simscape" model is selected. Introduced equations comprise the temperature effect which influences tremendously the battery performance. The battery role is instrumental to ensure microgrid stable operation by stabilizing the common DC bus voltage. The battery is modeled as a variable DC voltage source connected to common DC bus through a bidirectional DC/DC converter modeled as voltage source converter (VSC). The bidirectional DC/DC converter average model is adopted, and the equivalent electrical circuit diagram is identical to the DC/DC boost illustrated in Fig.2. b. The battery charging/discharging mode is identified from the inductor current sign:

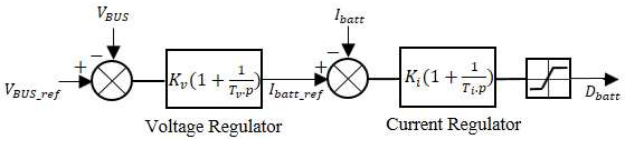


Fig.8 Battery cascaded loop control

- For $I_L > 0$, the converter is in boost mode and the battery is discharging to stabilize the common DC bus.
- For $I_L < 0$, the converter is in buck mode and the battery is charging to stabilize the common DC bus.

Bidirectional DC/DC average model equations are deduced as follows:

$$L\frac{dI_L}{dt} = V_{batt} - V_{Bus}.(1-D_b) - R_L.I_L \quad (7)$$

$$I_L.(1-D_b) - I_{BUS} = C_{BUS}\frac{dV_{BUS}}{dt} \quad (8)$$

$$I_L = I_{batt} \quad (9)$$

Where $L, I_L, V_{BUS}, D_b, V_{batt}, R_L, I_{BUS}, C_{BUS}$ and $I_{batt}$ are converter inductor, inductor current, common DC bus voltage, battery duty cycle ratio, battery voltage, inductor resistance, common DC bus current, common DC bus capacitor, and battery current. To stabilize the DC bus voltage the voltage and current cascaded loop regulation technique are adopted as shown in Fig.8. We take note that all mentioned P.I regulates in the paper are equipped with anti-windup systems.

However, variable DC current-sources are utilized to emulate the DC loads power consumption.

## III. THIRD CONTROL LEVEL POWER MANAGEMENT

In section II, the first and second control level of each unit source were detailed. In this section, a third control level is proposed to globally manage the Microgrid power flow. The third control level flow chart is shown in Fig.9. The management strategy is established based on two decision variables:

The first variable is the power balance between generated and demanded power and is equal to the sum of (RESs) generated power subtracted from the load consumption:

$$P_{Load} - \sum P_{sources} = P_{PV} + P_{PV} \quad (10)$$

the second variable is the battery state of charge (SOC) which must be limited in a certain interval to guarantee battery proper operation and prevent the excess discharge and overcharge.

$$SOC_{min} < SOC < SOC_{max} \quad (11)$$

When the SOC surpasses these thresholds, the battery performance, and lifetime are greatly decreased which impacts the whole microgrid stable operation and expands the maintenance cost.

As a principle, the proposed strategy starts by computing the first decision variable. If the generated power exceeds the load demand, then the $SOC$ variable is evaluated, and one of the two operating modes is selected. *Mode 1* ($SOC < SOC_{max}$): battery stabilizes the DC bus voltage by charging the surplus of unused power, the (DG) and grid are not connected to the microgrid

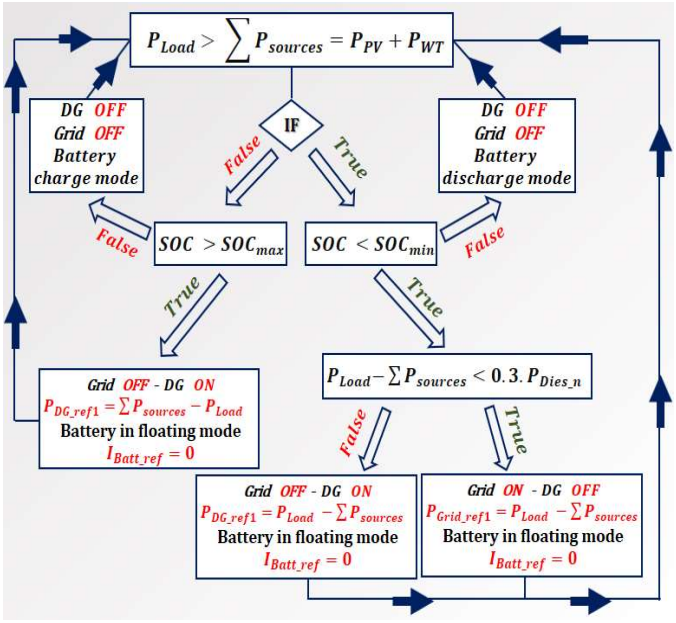


Fig.9 Third level control flow chart

which is operating in islanded mode. *Mode 2* ($SOC \geq SOC_{max}$): the battery already reached its higher admissible threshold, so it switches to a floating mode ($I_{batt} = 0$) and the surplus of power is sold to the grid. By this, the battery SOC is fixed on its threshold and the grid converter takes charge of stabilizing the DC bus voltage. On the other hand, if the load consumption is higher than power production then, the $SOC$ variable is compared to its minimum threshold and one of two operating modes is selected. *Mode 3* ($SOC > SOC_{min}$): battery stabilizes the DC bus voltage by discharging and supply the load with the unavailable needed power. The (DG) and gird are disconnected from the microgrid, operating in islanded mode. Yet, if ($SOC \leq SOC_{min}$) then, the power deficit must be covered either by the (DG) or by the utility grid. Standardly, DGs operate in a margin of (around 30%) to 100% of their nominal power. Hence, the existing power deficit is compared to the minimum admissible (DG) power generation. If it exceeds the 30% threshold then, the (DG) is turned on, connected to the microgrid, and generates unavailable power to cover the load needs. (DG) converter stabilizes the DC bus voltage (*mode 4)*. However, if the power deficit value is below the (DG) threshold, therefore the required power is purchased from the utility grid. Consequently, the utility grid converter takes charge of stabilizing the DC bus voltage and the microgrid operates in grid-connected mode (*mode 5)*. The proposed strategy sampling time is equal to $T_{sampling} = 20s$. Thus, the same control steps are restarted again after each period. Finally, we take note that (RESs) are considered as non-dispatchable units so they are operating continuously in MPPT mode to extract the maximum available power (second control level). Accordingly, they do not intervene in the third control level.

## IV. SIMULATION TESTS AND RESULTS

To prove the viability of the proposed 24-hour DC microgrid model along with the predefined hierarchical control, a realistic scenario, consisting of 24-hour sources and load profiles, is carried out. The effectiveness of the proposed model is assessed in terms of accuracy, complexity, and simulation speed. All system parameters are listed in table 1. 24-hour variable profiles are imposed. It comprises variable irradiance ($W/m^2$), air temperature (°C), wind speed ($m/s$), and load profiles ($W$). The DC microgrid power flow is shown in Fig.10. (RESs) generated power curves have the same form as their input profiles. The PV is operating in MPPT mode and reaches its maximum power generation: $P_{PV\_max} = 49.4\ KW$ corresponding to 1 $KW/m^2$ irradiance value at 12:30 P.M. However, the wind turbine applied characteristics are the same as defined in section II. It can be seen that a maximum wind generation is reached for a wind speed of 12 $m/s$ corresponding to $(0.9.P_{WT})$ → $P_{WT\_MPPT} = 0.9 \times 0.928 \times P_{WT\_n} = 45.94\ KW$.The wind turbine pitch controller intervenes when the wind speed exceeds 13.2 $m/s$ to limit the generated power on its allowable maximum rate $P_{WT\_max} = 0.91 \times 0.928 \times 55 = 46.45\ KW$. Thus, for higher wind speed values the wind power is limited at $P_{WT\_max}$. As seen in Fig.10 The saturation limit is reached twice in the simulation. On a third control level, all microgrid operating modes and transitions are summarized in table 2.

Nine operating mode transitions are envisaged in the 24-hour simulation: the (DG) is connected twice to the microgrid during peak load hours (Fig.10): (6:00 →8:00 & 17:30→20:00). Following the proposed power management strategy, each (DG) connection is succeeded by a grid connection when the microgrid power deficit drops bellow the (DG) minimum threshold. This management strategy is revealed in table 2 (transition to mode 5 is inevitably preceded by mode operation 4). By this, the (DG) and utility grid share the needed microgrid power production, which restricts the financial cost and environmental pollution. The DC bus voltage curve is shown in Fig.11, it is stabilized on its referenced value and does exceed its allowable limits is transient and steady-state. Hence, a seamless transition between different modes is stated along with a robust first and second control level regulators. Fig.12 comprises battery parameters. Battery SOC curve (Fig.12 (c)) shows convenient results in terms of modes transition and battery stable and safe operation. Practically, it operates within the predefined admissible boundaries $0.3 \leq SOC \leq 0.95$. Furthermore, a maximum variation of 10 °C, in battery cell temperature (Fig.12 (d)), is identified (16°C → 26°C) which highlights the necessity of including the temperature parameter in battery equations. Finally, the average calculation step size of the 24-hour assembled model is equal to 8.3 $ms$, which increases the simulation speed tremendously and reduces the usage of computer memory. A calculation step size ratio of 125 exists between the instantaneous model ***(included switching devices controlled by firing pulses )***and average model including ***(omitted switching devices, controlled by switching functions)*** $R_1 = \frac{1e^{-4}}{8e^{-7}} = 125$. Compared to the average model, the 24-hour proposed model has a further speed ratio of $R_2 = \frac{8.3\ e^{-3}}{1e^{-4}} = 83$. Finally, the wide range in step size variations of the "ode23tb (Stiff\TR-BDF2)" solver ($SS_{min} = 3e^{-30} \ll SS_{max} = 2.4$) made the proposed 24-hour model viable and found a best tradeoff between model accuracy and simulation speed improvement.

| | | |
|---|---|---|
| Common DC bus rated voltage | | $800\ V$ |
| Allowable DC bus voltage continuous deviation | | ± 10% |
| Allowable DC bus voltage fluctuation | | ± 5% |
| Wind turbine nominal power and efficiency (%) | | $55\ KVA$ - 92.8 % |
| PV array maximum rated power | | $50\ KW$ |
| (DG) Rated Parameters | Power (KW) - frequency (Hz) | $55\ KW$ - $50\ Hz$ |
| | Nominal voltage $V_n(ph-ph)$ | $367\ V$ |
| | $P_{DG\ min}\ (KW)$ | $16.5\ KW$ |
| Utility Grid Rated Parameters | Power (VA) - frequency (Hz) | $100\ VA$ - $50\ Hz$ |
| | Nominal voltage $V_n(ph-ph)$ | 380 V |
| | (P.I) current regulator coefficients | $K_{p\_G} = 9.93$<br>$K_{i\_G} = 3{,}1210.10^4$ |
| Battery rated capacity and voltage | | $500\ Ah - 250\ V$ |
| Battery minimum and maximum admissible (SOC) | | $SOC_{min} = 30\%$<br>$SOC_{max} = 95\%$ |
| (DG) (P.I) currents regulators coefficients | | $K_{p\_DG} = 8.68$<br>$K_{i\_DG} = 1{,}817.10^4$ |
| PV (I) boost power regulator coefficient | | $K_{i\_PV} = 3$ |
| (WT) (P. I) electrical power and current regulators coefficients | | $K_{p\_power} = 1$<br>$K_{i\_power} = 100$<br>$K_{p\_crt} = 3.42$<br>$K_{i\_crt} = 10752$ |
| Battery (P.I) voltage regulator coefficients | | $K_{p\_v} = 3{,}14.10^{-4}$<br>$K_{i\_v} = 0.0628$ |
| Battery (P.I) current regulator coefficients | | $K_{p\_c} = 6.2832$<br>$K_{i\_c} = 1{,}2484.10^4$ |

Table 1. DC microgrid parameters

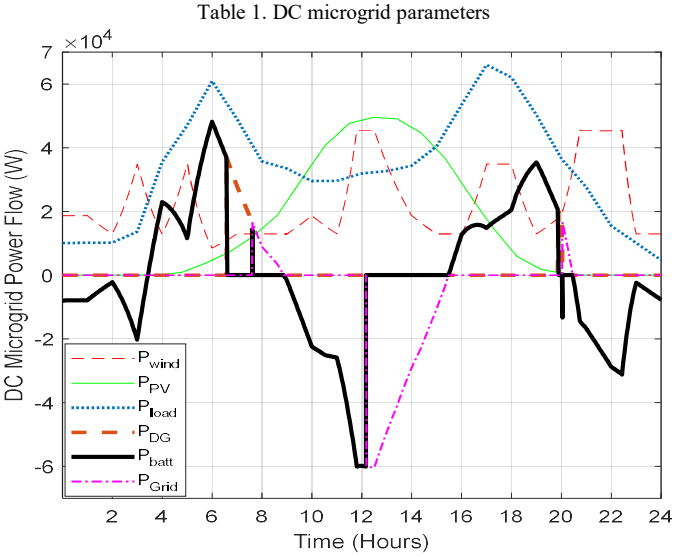


Fig.10 24-hour DC Microgrid Power Flow of operating Units (W)

| Operating mode | 1 | 3 | 4 | 5 | 1 | 2 | 3 | 4 | 5 | 1 |
|---|---|---|---|---|---|---|---|---|---|---|
| Start-End period (Hours) | 0 | 3.43 | 6.58 | 7.62 | 8.88 | 12.17 | 15.48 | 19.92 | 20.04 | 20.46 |
| | 3.43 | 6.58 | 7.62 | 8.88 | 12.17 | 15.48 | 19.92 | 20.04 | 20.46 | 24.00 |

Table 2. DC microgrid operating modes

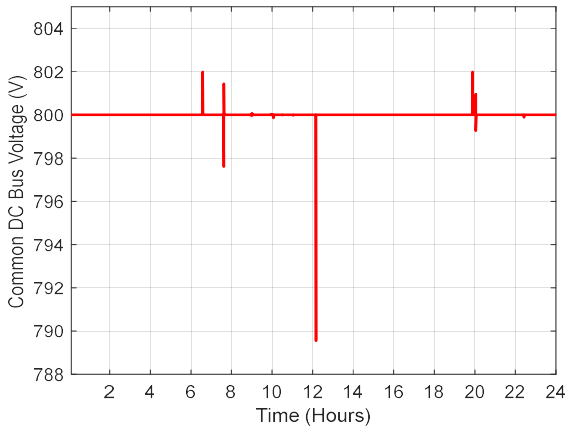


Fig.11 Common DC bus voltage and reference (V)

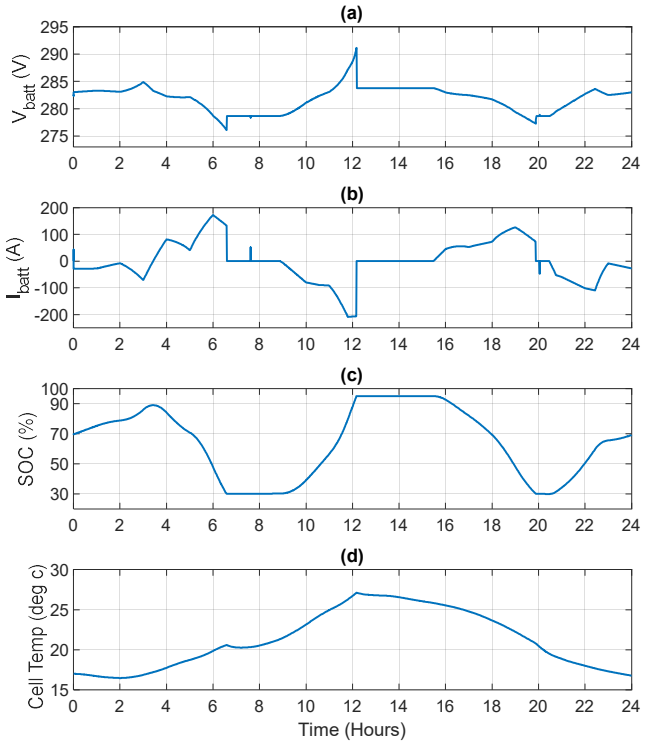


Fig.12. Battery (a) voltage (V), (b) current (A), (c) SOC (%), (d) cell temperature (℃ )

## V. CONCLUSION

In this paper, an improved 24-hour DC microgrid model is proposed with a multi-objective hierarchical control. The wide dynamic range of all existing system variables makes the 24-hour modelling subject a complicated matter in absence of high performant servers. To cope with this problem, modelling solutions are introduced to ensure the best tradeoff between model precision, complexity and simulation speed. On a first and second control level, a MPPT look-up table is adopted and compared to an instantaneous reference model. The phasor solution is applied to all AC microgrid units which highly improved the simulation speed and maintained the same model accuracy. Besides, all microgrid converters are modelled by their average equations and controlled directly by the duty cycle ratios which further reduced the model complexity. To test the viability of the proposed model, a third control level is added and different microgrid operating modes are introduced. Simulation tests were conducted on MATALB/Simulink platform. The obtained results prove the effectiveness of the proposed model in terms of accuracy (dynamic characteristics of system variables maintained), and simulation speed (a double speed ratio upgrade $R_1 = 125$, $R_2 = 83$).


## ACKNOWLEDGMENTS

The authors gratefully thank the PHC CEDRE Project No. 44529PH, the Lebanese National Council for Scientific Research (CNRS-L), and the Research Council of Saint-Joseph University for their financial support.


## REFERENCES


[1] A. Ipakchi and F. Albuyeh, "Grid of the future," *IEEE Power Energy Mag.*, vol. 7, no. 2, pp. 52–62, Mar. 2009.

[2] T. Dragičević, X. Lu, J. C. Vasquez, and J. M. Guerrero, "DC Microgrids—Part I: A Review of Control Strategies and Stabilization Techniques," *IEEE Trans. Power Electron.*, vol. 31, no. 7, pp. 4876–4891, Jul. 2016.

[3] L. Meng, T. Dragicevic, J. M. Guerrero, and J. C. Vásquez, "Optimization with system damping restoration for droop-controlled DC-DC converters," in *2013 IEEE Energy Conversion Congress and Exposition*, Sep. 2013, pp. 65–72.

[4] E. Hleihel, M. Fadel, and H. Y. Kanaan, "Simulation of an Islanded DC Microgrid Using Instantaneous and Average Modeling Approaches," in *ELECTRIMACS 2019*, Cham, 2020, pp. 193–207.

[5] H. A. Toliyat, "Analysis and simulation of multi-phase variable speed induction motor drives under asymmetrical connections," in *Proceedings of Applied Power Electronics Conference. APEC '96*, Mar. 1996, vol. 2, pp. 586–592 vol.2.

[6] M. A. Abdullah, A. H. M. Yatim, C. W. Tan, and R. Saidur, "A review of maximum power point tracking algorithms for wind energy systems," *Renew. Sustain. Energy Rev.*, vol. 16, no. 5, pp. 3220–3227, Jun. 2012.

[7] V. Akhmatov, "Variable-Speed Wind Turbines with Doubly-Fed Induction Generators, Part I: Modelling in Dynamic Simulation Tools," *Wind Eng.*, vol. 26, pp. 85–108, Mar. 2002.

[8] S. Benhamed *et al.*, "Dynamic modeling of diesel generator based on electrical and mechanical aspects," in *2016 IEEE Electrical Power and Energy Conference (EPEC)*, Oct. 2016, pp. 1–6.

[9] U. Mulleriyawage and W. Shen, "A Review of Battery Energy Storage Systems for Residential DC Microgrids and Their Economical Comparisons," *DEStech Trans. Environ. Energy Earth Sci.*, Feb.2019.

[10] E. Hleihel, M. Fadel and H. Y. Kanaan, "Control and Power Sharing of an Islanded DC Microgrid Integrating a Back-up Diesel Generator", in *Proc. 5th International Conference on Renewable Energies for Developing Countries (REDEC'20)*, Marrakech, Morocco, June 29-30, 2020, pp. 1-8.